JOURNAL OF Materials CHEMISTRY

Synthesis and structure of novel layered perovskite oxides: $Li_2La_{1.78}Nb_{0.66}Ti_{2.34}O_{10}$, and a new family, $Li_2[A_{0.5n}B_nO_{3n+1}]$

N. S. P. Bhuvanesh, M. P. Crosnier-Lopez, H. Duroy and J. L. Fourquet*

Laboratoire des Fluorures (UPRES A 6010, CNRS) Faculté des Sciences du Mans, Université du Maine, Avenue O. Messiaen, 72085 Le Mans Cedex 9, France. E-mail: jlf@fluo.univ-lemans.fr

Received 10th May 1999, Accepted 17th September 1999

Several new members ($n=2$, 3, 4 members) of the family of layered perovskites $Li_2[A_xB_nO_{3n+1}]$ (A = Ca, Sr, La; B = Nb, Ta, Ti, Fe) have been synthesized for the first time. The structure analysis of $Li_2SrNb_2O_7$ and $Li_2SrTa_2O_7$ determined by powder X-ray diffraction (XRD), and of $Li_2La_{1.78}Nb_{0.66}Ti_{2.34}O_{10}$ and $Li_2Sr_2Nb_{3.97}Fe_{0.03}O_{12.97}$ determined by single crystal XRD data, shows that these novel phases are related to the Ruddlesden–Popper series of compounds, $A'_2[A_{n-1}M_nO_{3n+1}]$. While the structures of $n=2$ members are identical to the RP series, in the higher members the A sites are partially occupied. Interestingly, the compounds for A = Ca, Sr and B = Nb, Ta, Fe indicate the formation of a new family of oxides of general formula $Li_2A_{0.5n}B_nO_{3n+1}$ where different members of the family can be synthesized with the same set of A and B atoms.

Ruddlesden–Popper (RP) compounds ($A'_2[A_{n-1}B_nO_{3n+1}]$),[1–3] Dion–Jacobson (DJ) series ($A'[A_{n-1}B_nO_{3n+1}]$),[4–9] layered brownmillerites ($(A'[A_{n-1}B_nO_{3n+1-\delta}])$[10] and the Aurivillius phases (Bi_2O_2)[$A_{n-1}B_nO_{3n+1}$])[11] form the major families of closely related layered perovskites. Fig. 1 shows the relation between the different series for a typical $n=3$ member. Thus, with a knowledge of structural relationship, it is possible to design the synthesis of several members of these perovskite related compounds. Examples of such design are shown by the evidence of formation of layered brownmillerite, $ACa_2Nb_2AlO_9$,[10] and also by suitable substitution, the bridging of the RP and the DJ series in the A–La–Nb–Ti–O system.[12] There is always a look-out for new members of these families because of the interesting properties they exhibit such as ion-exchange and intercalation,[4–9,13–15] ionic conductivity,[16,17] photocatalysis,[18–20] ferromagnetic and magnetoresistive properties[21–23] and also superconductivity.[24]

Recently, we have reported[25,26] syntheses, crystal structures and ionic conductivities of some novel members of the series $Li_2[A_xB_nO_{3n+1}]$ ($n=3$ for A = Sr; B = Nb, Fe and $n=2$ and 4 for A = La; B = Nb, Ti). We also evidenced[27] interesting irreversible electron-induced structural transformation during our high-resolution electron microscopic studies, involving a change from a tetrahedral to an octahedral environment around lithium with a significant decrease in the *c*-parameter, in these phases. During our investigations of these phases we found indications for the formation of other members of the system (*i.e.*, $n=2$, 4 in the Li–Sr–Nb–Fe–O system and $n=3$ for the Li–La–Nb–Ti–O system). Here we report the synthesis and structural characterisation of the novel phases $Li_2A_{0.5n}(B_{n-x}Fe_x)O_{3n+1}$ (for $n=2$ and 4; A = Ca, Sr; B = Nb, Ta) and $Li_2La_{1.78}(Nb_{0.66}Ti_{2.34})O_{10}$. The significance of this study is that the former compounds of the Li–Sr–Nb–Fe–O system correspond to a new family of layered perovskites, $Li_2A_{0.5n}(B_{n-x}Fe_x)O_{3n+1-x}$ (for $n=2$, 3, 4; A = Ca, Sr; B = Nb, Ta), which are closely related to RP compounds, where members with different *n* values could be prepared with the same set of A and B cations, which consequently leads to an increase in A site deficiency in higher members.

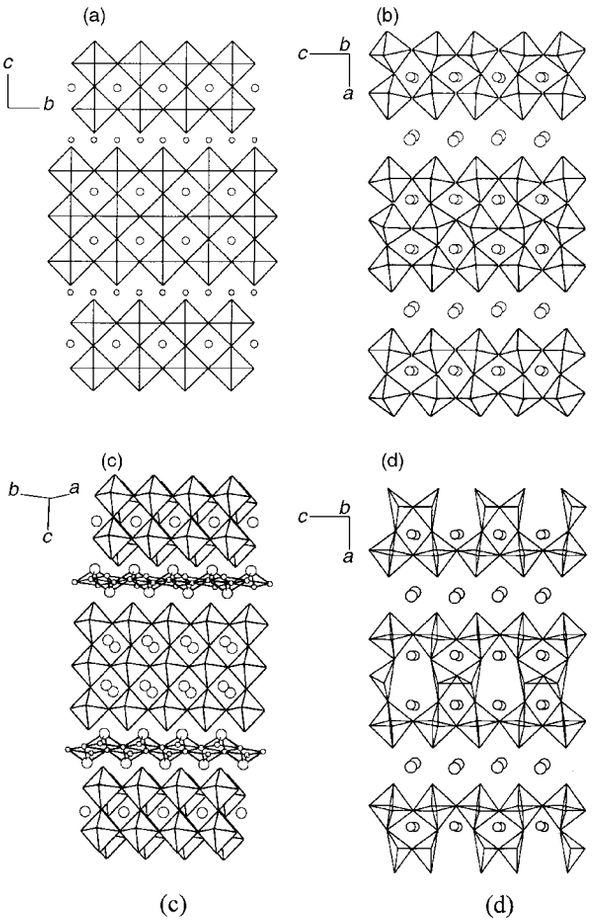

Fig. 1 Structure of various well known layered perovskite families, (a) Ruddlesden–Popper (the interlayer sites fully occupied), (b) Dion–Jacobson (with the interlayer space half occupied), (c) Aurivillius (square-pyramidal Bi_2O_2 sheets forming the interlayer) and (d) layered brownmillerite phases (with an ordering of vacancies in the perovskite layer), for typical $n=3$ members.

Table 1 Composition and preparation conditions[a] for the polycrystalline samples, $Li_2A_{0.5n}(Nb_{n-x}Fe_x)O_{3n+1-x}$

Composition	n	Amount of excess Li_2CO_3 (mol%)	Final heating temperature/°C	Heating duration/h
$Li_2SrNb_2O_7$	2	10	1050	96[b]
$Li_2SrTa_2O_7$	2	10	1250	12
$Li_2Ca_{1.5}Nb_3O_{10}$	3	10	1050	6
$Li_2Sr_2(Nb_{3.75}Fe_{0.25})O_{12.75}$	4	25	1200	24

[a]For all the compounds a heating rate of 5 °C min^{-1} and a natural cooling is used. [b]With three intermittent grindings.

Synthesis

The synthesis of the different compounds of the series requires very critical conditions in terms of starting composition, temperature, and cooling rate, owing to the volatility of the lithium oxide at higher temperatures. Table 1 lists the conditions of preparation of polycrystalline samples of the series $Li_2A_{0.5n}(B_{n-x}Fe_x)O_{3n+1-x}$ (for $n=2$, 3, 4; A = Ca, Sr; B = Nb, Ta, Fe). All the compositions were preheated at 550 °C before the final heating temperature. Excess Li_2CO_3 (Table 1) was used to compensate for the volatility of Li_2O at higher temperature.

Single crystals of $Li_2La_{1.78}(Nb_{0.66}Ti_{2.34})O_{10}$ ($n=3$ member of the Li–La–Nb–Ti–O system) were selected from a product obtained by heating Li_2CO_3, La_2O_3 (preheated to 1000 °C for 12 h), Nb_2O_5 and TiO_2 in the molar proportion 3.75 : 1.5 : 1.0 : 2.0 at 850 °C for 12 h and at 1050 °C for 6 h followed by cooling at 0.5 °C min^{-1}.

Pale brown single crystals of $Li_2Sr_2Nb_{3.97}Fe_{0.03}O_{12.97}$ ($n=4$ member of the Li–Sr–Nb–Fe–O system) were obtained as platelets by heating Li_2CO_3, $SrCO_3$, Nb_2O_5 and Fe_2O_3 in the molar ratio 0.35 : 0.30 : 0.425 : 0.075 first at 850 °C for 6 h and then at 1050 °C for 12 h. Then a final heating† was performed at 1200 °C for 24 h followed by a cooling at 0.3 °C min^{-1} to room temperature.

Structural analysis

$Li_2SrNb_2O_7$ ($n=2$)

Samples of $Li_2SrNb_2O_7$ were characterised by powder X-ray diffraction recorded on a Bruker D8 Advance diffractometer at room temperature (Cu-Kα radiation) in the 2θ range 5–130° with a step scan, $\Delta 2\theta = 0.01$, and a step time of 35 s. The XRD patterns were analyzed by the Rietveld method using the FULLPROF program.[28] Major peaks of the pattern (in the 2θ range 20–70°) could be indexed on a tetragonal cell with $a=3.9581(1)$, $c=18.012(6)$ Å and the systematic absences showing body centering leading to the extinction symbol $I---$. Thus, we attempted to refine the structure in the space group $I4/mmm$ with a starting model similar to $Li_2LaNb_2O_7$.[29] For the refinement, with 19 parameters for 228 reflections, we found the conventional reliability factors, R_p, R_{wp}, R_{exp}, R_B and R_F to be 22.0, 22.3, 10.18, 9.40 and 6.73%, respectively.

We found that some of the reflections in the region above $2\theta = 80°$ were split which could not be explained by the above model. Efforts to index the pattern, including the split reflections, using a larger tetragonal unit cell were not successful, while we found finally that all the reflections were well indexed in an orthorhombic cell [$a=5.5939(1)$, $b=5.6013(1)$, $c=18.011(3)$ Å]. The systematic absences appear to lead to a $F---$ extinction symbol, but our calculations in the $Fmmm$ space group were not completely satisfactory ($R_p=17.4\%$) (Table 2). While the heavy atoms are probably well located in our model, the X-ray powder data cannot allow a precise determination of the oxygen atom positions. As already encountered in such compounds, a small displacement of these oxygen atoms leading to a tilting of the octahedra could not be revealed by the powder X-ray diffraction study. Indeed, we were informed at the end of this work that Floros *et al.*[30] have carried out structural work on $Li_2SrNb_2O_7$ and $Li_2SrTa_2O_7$, based on powder neutron diffraction experiments. For $Li_2SrNb_2O_7$, their work shows the same super cell and the octahedra tilting in the orthorhombic system (space group $Cmcm$). These results are published in the following paper.

Table 2 Crystallographic characteristics for $Li_2SrNb_2O_7$ in the space group $Fmmm$ (no. 69)[a]

Atom	Site	x	y	z	B/Å^2
Nb	8i	0	0	0.38456(3)	0.17(1)
Sr	4a	0	0	0	0.71(3)
O1	16j	1/4	1/4	0.1073(2)	1.73(7)
O2	8i	0	0	0.2855(3)	1.73(7)
O3	4b	0	0	1/2	1.73(7)
Li	8f	1/4	1/4	1/4	0.7(3)

[a]$a=5.5939(1)$, $b=5.6013(1)$, $c=18.011(3)$ Å. 358 reflections and 21 parameters were used for refinement. $R_p=17.4\%$, $R_{wp}=19.2\%$, $R_{exp}=10.11\%$, $R_B=6.21\%$, $R_F=4.62\%$. B values are taken to be the same for all the oxygen atoms. Owing to high asymmetry, the first peak at $2\theta=9.974°$ was not taken into consideration in the refinement.

$Li_2SrTa_2O_7$ ($n=2$)

We were interested in synthesizing the tantalum analog of $Li_2SrNb_2O_7$, *viz.*, $Li_2SrTa_2O_7$, to investigate if similar problems would exist in the latter compound. For this compound we did not observe the splitting encountered in $Li_2SrNb_2O_7$, which was in disagreement with the results of Floros *et al.*[30] We could index the powder X-ray diffraction‡ pattern in a tetragonal cell [$a=3.9499(2)$, $c=18.200(3)$ Å]. Rietveld refinement of the diffraction pattern in the space group $I4/mmm$ (Fig. 2) converged to $R_p=11.3\%$, $R_{wp}=12.0\%$, $R_{exp}=1.77\%$, $R_B=4.72\%$ and $R_F=3.85\%$ (Table 3).

Single crystal analysis

Single crystals of $Li_2La_{1.78}(Nb_{0.66}Ti_{2.34})O_{10}$ and $Li_2Sr_2Nb_{3.97}Fe_{0.03}O_{12.97}$ were first examined by standard precession X-ray photographic methods. The experimental conditions for the collection of X-ray diffraction (XRD) data are listed in Table 4. The lattice parameters [$a=5.4730(23)$ ($\approx\sqrt{2}a_p$), $c=26.331(17)$ Å for the former and $a=3.9609(7)$, $c=33.821(6)$ Å for the latter] were refined by a double scan technique from the position of 28 reflections in the vicinity of $2\theta=30°$. Four-circle single-crystal diffractometer data were analyzed with the SHELX-93 program[31] and atomic scattering factors, $\Delta f'$ and $\Delta f''$ for the cations were taken from ref. 32. For O^{2-} the above values were taken from ref. 33.

†It should be noted that single crystals of $Li_4Sr_3Nb_{5.77}Fe_{0.23}O_{19.77}$ ($n=3$) are obtained[25] if the final heating at 1200 °C is performed for 12 h followed by a 2 °C min^{-1} cooling rate. The reason for this is the fact that, while the ratio of Sr to Nb/Fe nearly remains the same for both $n=3$ and 4 compounds, the ratio of Sr and Nb/Fe, on the one hand, and Li, on the other, is different. Therefore slower cooling leads to more loss in Li and eventually results in the $n=4$ compound.

‡Unless mentioned otherwise, all the powder X-ray diffraction patterns were recorded on a D-500 Siemens diffractometer at room temperature in the 2θ range 5–130° with a step scan $\Delta 2\theta=0.02°$, step time = 30 s.

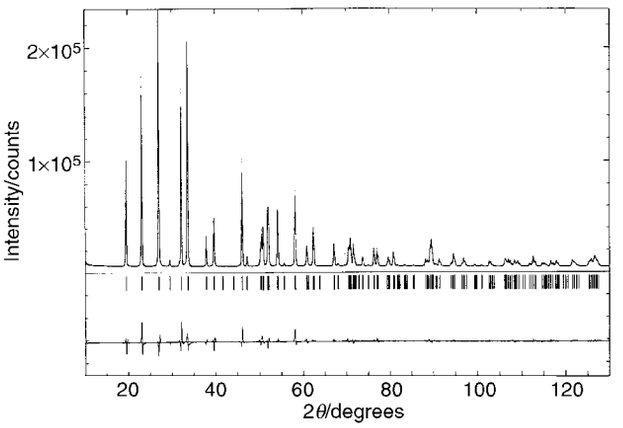

Fig. 2 Observed (····), calculated (—) and difference powder X-ray diffraction profiles of $Li_2SrTa_2O_7$ in the *I*4/*mmm* space group.

Table 3 Crystallographic characteristics for $Li_2SrTa_2O_7$ in the space group *I*4/*mmm* (no. 139)[a]

Atom	Site	*x*	*y*	*z*	*B*/Å^2
Ta	4e	0	0	0.38532(6)	0.60(1)
Sr	2a	0	0	0	1.01(4)
O1	8g	0	1/2	0.1014(4)	1.1(3)
O2	4e	0	0	0.2817(5)	1.1(3)
O3	2b	0	0	1/2	1.1(3)
Li	4d	0	1/2	1/4	2.6(8)

[a] $a=3.9499(2)$, $c=18.200(3)$ Å. 100 reflections and 20 parameters were used for refinement. $R_p=11.3\%$, $R_{wp}=12.0\%$, $R_{exp}=1.77\%$, $R_B=4.72\%$, $R_f=3.85\%$. *B* values are taken to be the same for all the oxygen atoms. Owing to high asymmetry, the first peak at $2\theta=9.801°$ was not taken into consideration in the refinement.

Full crystallographic details, excluding structure factors, have been deposited at the Cambridge Crystallographic Data Centre (CCDC). See Information for Authors, 1999, Issue 1. Any request to the CCDC for this material should quote the full literature citation and the reference number 1145/184.

$Li_2La_{1.78}(Nb_{0.66}Ti_{2.34})O_{10}$ ($n=3$)

A crystal of approximate size $0.152\times0.228\times0.046$ mm with natural boundary faces $\pm\langle110\rangle$, $\langle1\bar{1}0\rangle$ and $\langle001\rangle$ was selected for the X-ray diffraction data collection (Table 4). A careful examination of the intensity data showed the systematic absences ($h+k=2n+1$ for $hk0$ reflections and $l=2n+1$ for $0kl$ reflections) characteristic of the extinction symbol *Pnc*− compatible only with the space group $P4_2/ncm$ (no. 138). The Patterson method was used to elucidate the initial positions of the heavy atoms (La, Nb and Ti) and gave a starting model with three cationic sites. The remaining atom positions were revealed by successive Fourier difference synthesis: seven anionic sites and finally two sites for Li^+ ions. Two half occupancy oxygen atoms, O6 and O7, occupying 8g and 8i sites, respectively, were located. Allowing the occupancy of La atoms and the statistical distribution of Nb^{5+} and Ti^{4+} atoms over their two possible sites [8i for (Nb, Ti)1 and 4d for (Nb, Ti)2] to be refined, we found the *R* factor decreased rapidly. For the final stage of refinement, all the atoms were refined anisotropically (except for Li^+ ions) and, with absorption correction, weighting scheme, secondary extinction and 59 refined parameters, the *R* values converged to $R=0.0354$ for 496 data with $F_o>4\sigma(F_o)$, 0.0788 for all the 920 data. The final Fourier difference synthesis was featureless with maxima and minima close to ±2.5 e Å^{-3} and located near heavy atoms [La, (Nb, Ti)1 and (Nb, Ti)2].

At this stage, the final formula obtained, $Li_2La_{1.78}(Nb_{0.66}Ti_{2.34})O_{10}$, was supported by an electron microprobe analysis which gives an atomic ratio La : Nb : Ti of 2.7 : 1 : 3.5. It should be pointed out that several oxygen atoms exhibited anomalously small temperature factors at the completion of the refinement. The fractional atomic coordinates and thermal parameters are listed in Table 5.

Interestingly, we found all the observed reflections leading to the super cell $\sqrt{2}a_p$ (*hkl* with *h* or *k* odd) were very weak (the most intense of this set had a relative intensity of $<1\%$ of the strongest reflection). If we neglect these weak reflections, the structure could be considered in the sub-cell with a ($\approx a_p$) $=3.8701(12)$, $c=26.330(17)$, with systematic absences $h+k+l=2n+1$, leading to the extinction symbol $I---$. Refinement of the structure in the *I*4/*mmm* space group using the model of $Li_2Sr_{1.5}Nb_3O_{10}$, reported from our laboratory,[25] for heavy atom sites and successive Fourier difference synthesis led to the complete structure and the reliability factor *R* converged to 0.0259 for 315 data with $F_o>4\sigma(F_o)$, 0.0273 for all 323 data with 27 refined parameters. It is of note that the anisotropic and isotropic thermal factors had meaningful values for all the atoms.

$Li_2Sr_2Nb_{3.97}Fe_{0.03}O_{12.97}$ ($n=4$)

The standard crystallographic analysis for $Li_2Sr_2Nb_{3.97}Fe_{0.03}O_{12.97}$ suggested a tetragonal symmetry ($a\approx3.9$,

Table 4 Crystallographic parameters and operating conditions for the X-ray data collection[a] and refinement

	$Li_2La_{1.78}Nb_{0.66}Ti_{2.34}O_{10}$	$Li_2Sr_2Nb_{3.97}Fe_{0.03}O_{12.97}$
Symmetry	Tetragonal	Tetragonal
Space group	$P4_2/ncm$ (no. 138)	*I*4/*mmm* (no. 139)
$a(=b)$/Å	5.4730(23)	3.952(1)[c]
c/Å	26.331(17)	33.746(1)
V/Å^3	788.70	527.06
Z	4	2
M	594.98	765.56
T/°C	20	20
Absorption coefficient, μ/cm^{-1}	117.33	139.40
Reflections measured		
Total	4151 (210 standards)	9926 (579 standards)
Used in refinement	496	171
Number of refined parameters	59	32
Weighting scheme[b]	$A=0.0497$, $B=0.02$	$A=0.932$, $B=0.00$
Electron density in final Fourier difference map: max., min./e Å^{-3}	2.50, −1.40	2.78, −1.61
R_1 [for $F_o>4\sigma(F_o)$] and for all data	0.0354, 0.0788	0.0582, 0.1015

[a] The single crystal X-ray diffraction data for $Li_2La_{1.78}Nb_{0.66}Ti_{2.34}O_{10}$ and $Li_2Sr_2Nb_{3.97}Fe_{0.03}O_{12.97}$ were collected on Siemens AED2 and Nonius CAD4 diffractometers respectively with Mo-Kα graphite monochromated radiation ($\lambda=0.70926$ Å). Absorption corrections were applied using the Gaussian method. [b] $w=1/[\sigma^2(F_o^2)+(AP)^2+BP]$, where $P=1/3[\mathrm{Max.}(F_o^2,0)+2F_c^2]$. [c] Although the analysis of the data was made with this *a* parameter, the data were collected in a larger cell ($a'=\sqrt{2}a$).

Table 5 Fractional atomic coordinates and isotropic thermal parameters U_{eq} for $Li_2La_{1.78}(Nb_{0.66}Ti_{2.34})O_{10}$

Atom	x	y	z	SOF[a]	$U_{eq}/10^4$ Å^2
Nb1	0.5016(1)	0.5016(1)	0.15832(2)	0.31(1)	102(2)
Ti1	0.5016(1)	0.5016(1)	0.15832(2)	0.69(1)	102(2)
Nb2	0.0	0.0	0.0	0.04(1)	102(4)
Ti2	0.0	0.0	0.0	0.96(1)	102(4)
La	0.4972(1)	0.0028(1)	0.07962(1)	0.86(1)	119(2)
O1	0.25	0.25	0.1488(4)	1	167(22)
O2	0.0112(5)	0.4888(5)	0.2740(2)	1	179(8)
O3	0.0189(7)	0.0189(7)	0.0720(2)	1	211(10)
O4	0.75	0.75	0.1381(3)	1	48(12)
O5	0.75	0.25	0.1478(3)	1	147(17)
O6	0.1918(14)	0.6918(14)	0.0	0.5	109(21)
O7	0.2845(19)	0.2155(19)	0.9945(5)	0.5	212(37)
Li1	0.75	0.75	0.2563(6)	1	193(19)
Li2	0.75	0.25	0.25	1	193(19)

[a]SOF = Site occupancy factor.

$c \approx 33.8$ Å) with *4/mmm* Laue class and systematic absences leading to an extinction symbol $I- - -$.

A crystal of approximate dimensions $0.019 \times 0.28 \times 0.133$ mm with natural boundary faces $\pm\langle 001\rangle$, $\pm\langle 100\rangle$ and $\langle 010\rangle$ was selected for the XRD data collection (Table 4). Though the lattice parameters obtained for this compound were $a = 3.9609(7)$, $c = 33.821(6)$ Å, we collected the XRD data in a larger cell with $a = 5.6016(9)$, $c = 33.821(6)$ Å, since it is known that a similar compound, $Li_2La_{2.25}Nb_{1.25}Ti_{2.75}O_{13}$, reported from our laboratory[26] crystallizes in the space group *P4/mmm* (no. 136), showing very weak reflections which lead to a tetragonal cell, $a = 5.4915(6)$, $c = 33.812(4)$ Å. As the data indicated no reflections which could define a larger cell, we went ahead with the structure analysis in the cell: $a = 3.9609(7)$, $c = 33.821(6)$ Å with a transformation. The systematic absences lead to the extinction symbol $I- - -$ and the possible space groups *I*422 (no. 97), *I4mm* (no. 107), $I\bar{4}m2$ (no. 119), $I\bar{4}2m$ (no. 121) and *I4/mmm* (no. 139). (It should be pointed out here that we found some weak reflections, the intensity of which was $<1\%$ of the strongest, which could not be accounted for with this extinction symbol, an analysis of systematic absences including these weak reflections did not yield us any possible extinction symbols.) We could get a good starting model in the space group *I4/mmm* which led us to the position of one heavy atom Nb^{5+}, and subsequent Fourier difference synthesis resulted in one Nb^{5+}, two Sr^{2+}, five anionic (O^{2-}) and finally one position for Li^+ (Table 6). We found that the Sr^{2+} positions (4e and 2b sites) are partially occupied. Also allowing Fe^{3+} to distribute in the Nb^{5+} sites we found the *R* factor decreased to a reasonable value. Allowing all the atoms to be refined anisotropically (except Li^+) and with absorption correction, weighting scheme, secondary extinction and 32 refined parameters, the *R* values converged to $R = 0.0573$ for 171 data with $F_o > 4\sigma(F_o)$, and 0.0879 for all the 194 data. The final Fourier difference synthesis was featureless with maxima and minima close to ± 2.6 e Å^{-3} located near heavy atoms. Tests with other possible space groups did not improve the results.

Electron microscopy

Transmission electron microscopic (TEM) studies, electron diffraction (ED) and high resolution electron imaging (HREM), were carried out with a JEOL 2010 electron microscope operating at 200 kV and equipped with a side entry $\pm 30^\circ$ double tilt specimen holder.

$Li_2SrNb_2O_7$ (polycrystalline) and $Li_2Sr_2Nb_{3.97}Fe_{0.03}O_{12.97}$ (single crystals) were taken for microscopic studies. Samples were crushed under *n*-butanol in an agate mortar. A drop of the resulting suspension was then placed on a Cu grid with a holey carbon film and the grid allowed to dry before examination. For the two phases, the electron diffraction study was performed on several crystallites and reconstruction of the reciprocal space was performed. HREM imaging was done with the electron beam parallel to the perovskite slabs which gives the best description of the atomic stacking in this kind of compound.

$Li_2SrNb_2O_7$

Scanning of the reciprocal space for some of the crystallites allowed us to determine the cell parameters ($a \approx a_p \approx 3.9$ Å, $c = 18.0$ Å), where a_p represents the cell parameter for a cubic perovskite) with systematic absences leading to the conclusion of a body centered cell. Some of the crystallites, nevertheless, clearly show additional spots which lead to a larger cell: $a \approx \sqrt{2}a_p \approx 5.5$ Å and $c \approx 18.0$ Å (Fig. 3). We found, however, that the determination of the exact extinction symbol, in the latter case, was difficult.

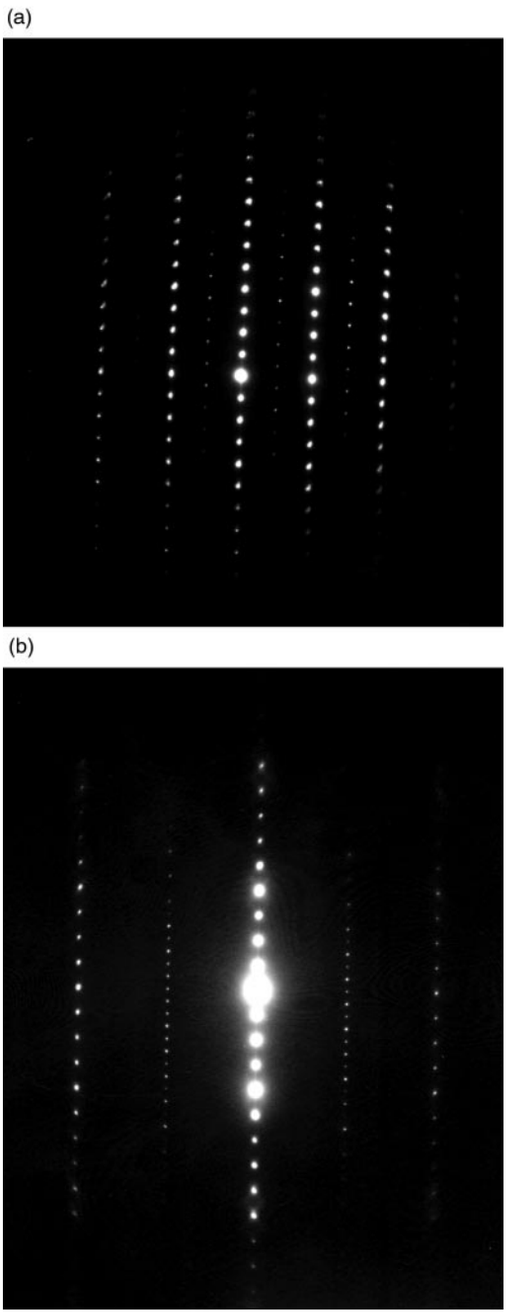

Fig. 3 SAED patterns of $Li_2SrNb_2O_7$ in (a) [010] and (b) $[2\bar{1}0]$ zone axes showing weak spots which would lead to a larger cell: $a \approx \sqrt{2}a_p$.

Table 6 Fractional atomic coordinates and isotropic thermal parameters U_{eq} for $Li_2Sr_2Nb_{3.97}Fe_{0.03}O_{12.97}$

Atom	x	y	z	SOF[a]	$U_{eq}/10^4$ Å^2
Sr1	0.0	0.0	0.61787(9)	0.82(1)	9(1)
Sr2	−0.5	−0.5	0.0	0.43(1)	5(2)
Nb1	0.0	0.0	0.05825(5)	0.98(1)	8(1)
Fe1	0.0	0.0	0.05825(5)	0.02(1)	8(1)
Nb2	0.0	0.0	0.17867(6)	1	6(1)
O1	0.0	0.0	0.0	1	15(6)
O2	0.0	0.0	0.1155(5)	1	23(5)
O3	0.0	0.0	0.2339(5)	1	6(3)
O4	0.0	−0.5	0.05968(3)	1	15(3)
O5	0.0	−0.5	0.17349(4)	1	10(2)
Li1	−0.5	0.0	0.25000	1	1(1)

[a]SOF = Site occupancy factor.

HREM investigations show that the crystals are well ordered with a regular contrast. Some of the crystallites also showed defects with domains of an $n=3$ member interleaving the $Li_2SrNb_2O_7$ matrix (Fig. 4).

$Li_2Sr_2Nb_{3.97}Fe_{0.03}O_{12.97}$

All the crystallites of $Li_2Sr_2Nb_{3.97}Fe_{0.03}O_{12.97}$ exhibit electron diffraction patterns with two sets of spots, intense and weak. While all the intense spots could be indexed with a tetragonal cell: $a \approx a_p \approx 3.9$ Å, $c \approx 33.8$ Å, showing a body centered cell, we could account for the weak spots only with a larger tetragonal cell $a \approx \sqrt{2}a_p \approx 5.5$ Å and $c \approx 33.8$ Å, with the systematic absences, $hk0$, $h+k=2n$, $h0l$, $h+l=2n$, leading to the space group $P4_2/nnm$. Fig. 5 shows three different sections of the reciprocal space. Most of the SAED patterns showed diffuse streaks parallel to the c axis, indicating a stacking disorder along this direction. Indeed, HREM imaging (Fig. 6) of these crystallites reveals intergrowth of different higher members ($n=5$ and 7).

In both the compounds, we observed an irreversible structural change under the electron beam similar to other members of the Li–La–Nb–Ti–O ($n=2$, 3, 4) and Li–Sr–Nb–Fe–O ($n=3$) systems reported by us.[27] The transformation involved a shrinking of the c parameter and leading to the space group $I4/mmm$. We have attributed these changes,[27] in the other members, as due to a straightening up of the octahedra and a change in the Li^+ coordination which changes to octahedral from tetrahedral. While all other members studied by us in the Li–La–Nb–Ti–O and Li–Sr–Nb–Fe–O systems[27] have vacancies in the twelve-coordinated perovskite cages, $Li_2SrNb_2O_7$ does not have any vacant sites. Thus, we conclude that the structural modification, under the electron beam used for high resolution, is not due to movement of the Li^+ ions from vacant twelve-coordinate sites to the interlayer regions, but rather is caused by the straightening of the BO_6 octahedra and decrease in c with the change in the Li^+ coordination.

Fig. 4 [100] HREM image for $Li_2SrNb_2O_7$ showing domains of an $n=3$ member interleaving the parent matrix.

Discussion

The structures (Fig. 7) of the various members investigated by us are closely related to the RP phases. Although the structures

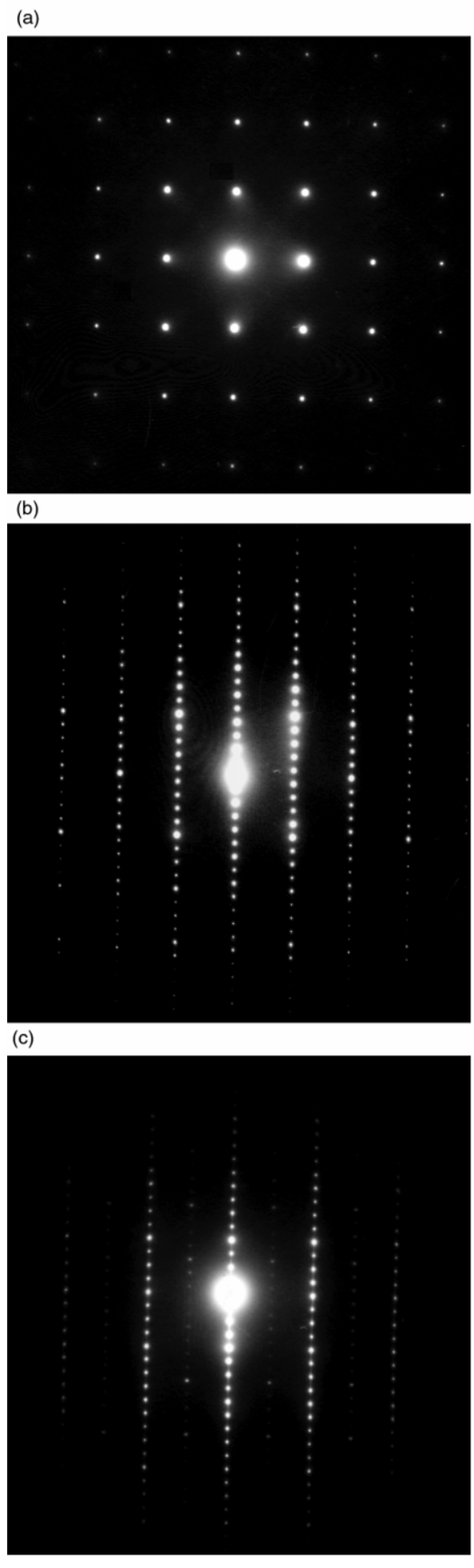

Fig. 5 Typical SAED patterns of $Li_2Sr_2Nb_{3.97}Fe_{0.03}O_{12.97}$ in (a) [001], (b) [1$\bar{1}$0] and (c) [010] zone axes.

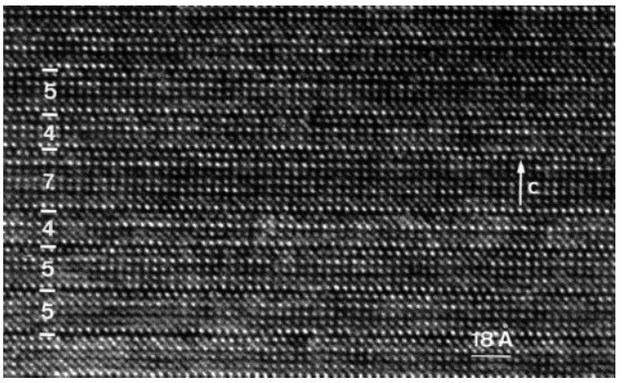

Fig. 6 A section of an HREM image of $Li_2Sr_2Nb_{3.97}Fe_{0.03}O_{12.97}$ clearly showing the intergrowth of higher members ($n=5$ and 7).

of the $n=2$ members, *viz.*, $Li_2SrNb_2O_7$ and $Li_2SrTa_2O_7$, are identical to the corresponding members of the RP series, we find that the twelve-coordinated A sites are partially occupied in the higher members ($n=3$ and 4). The structures of all the $Li_2[A_xB_nO_{3n+1}]$ compounds discussed here can be defined as formed by cutting the perovskite structure with a slab thickness of n BO_6 (B = Nb, Ti, Fe) octahedra with the alternate layers shifted by $(a+b)/2$ along (001). The larger A (La, Sr) atoms either fully or partially occupy the twelve-coordinated perovskite cages. The lithium atoms find themselves tetrahedrally coordinated and interleaved in-between the slabs. Surprisingly, while $Li_2SrTa_2O_7$ refines in *I*4/*mmm* space group, we found that for $Li_2SrNb_2O_7$, a split in the reflections at higher angles could only be explained with a larger cell, $a \approx b \approx \sqrt{2}a_p$, $c=18.0118(1)$ Å, the latter probably caused by a tilting of the NbO_6 octahedra.[30] On the other hand, our HREM imaging of $Li_2SrNb_2O_7$ clearly indicates the presence of defects in some of the crystallites. These defects can be explained as due to the formation of small domains of a higher member ($n=3$) in a matrix of the predominant phase. The formation of such intergrowth structures is well known in such layered perovskites, *e.g.*, in the $SrTiO_3$–SrO system.[34]

For $Li_2La_{1.78}Nb_{0.66}Ti_{2.34}O_{10}$, some of the very weak reflections with $h+k=2n+1$ for $hk0$ and $l=2n+1$ for $0kl$ indicate a possible space group as $P4_2/ncm$, and analysis without these reflections led us to the *I*4/*mmm* space group. Similar analysis without the weak reflections defines the space group for $Li_2Sr_2Nb_{3.97}Fe_{0.03}O_{12.97}$ as *I*4/*mmm*. The very weak reflections in the latter two phases, observed in the single crystal X-ray diffraction data, are probably due to either a small turbostratic stacking of the perovskite slabs or intergrowth of other members of the series, as observed for $Li_2SrNb_2O_7$. We see evidence for the intergrowth of higher members ($n=5$ and 7) in the HREM images of $Li_2Sr_2Nb_{3.97}Fe_{0.03}O_{12.97}$. Similar very weak reflections have also been reported, but have not been considered, in the single crystal analysis of $Na[NaCa_2Nb_3O_{10}]$ which belongs to the related DJ family of layered perovskites.[35]

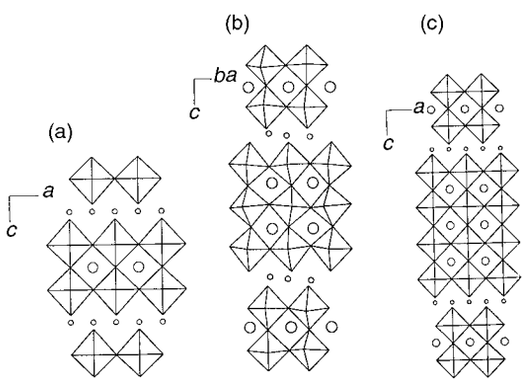

Fig. 7 Structure of RP related compounds, (a) $Li_2SrNb_2O_7$ ($n=2$), (b) $Li_2La_{1.78}Nb_{0.66}Ti_{2.34}O_{10}$ ($n=3$) and (c) $Li_2Sr_2Nb_{3.97}Nb_{0.03}O_{12.97}$ ($n=4$). In (b) and (c) the twelve-coordinated perovskite cages are partially occupied.

Table 7 Main bond distances for $Li_2SrTa_2O_7$

Ta–O/Å	Sr–O/Å	Li–O/Å
$1\times1.886(9)$	$8\times2.703(4)$	$4\times2.058(2)$
$4\times1.990(1)$	$4\times2.793(1)$	
$1\times2.087(1)$		

Table 8 Selected interatomic distances (Å) and angles (°) for $Li_2La_{1.78}(Nb_{0.66}Ti_{2.34})O_{10}$

$(Nb,Ti)1O_6$ octahedron

(Nb,Ti)1	O2	O5	O5	O1	O4	O3
O2	*1.783(4)*	2.827(5)	2.827(5)	2.867(6)	2.961(6)	4.061(7)
O5	98.2(3)	*1.955(1)*	3.870(6)	2.737(0)	2.748(1)	2.784(7)
O5	98.2(3)	163.6(3)	*1.955(1)*	2.737(0)	2.748(0)	2.784(7)
O1	99.7(3)	88.6(1)	88.6(1)	*1.964(1)*	3.880(7)	2.700(9)
O4	103.1(3)	88.2(1)	88.2(1)	157.2(3)	*1.995(2)*	2.714(7)
O3	178.4(4)	81.8(3)	81.8(3)	78.6(4)	78.5(4)	*2.279(4)*

$\langle$(Nb,Ti)1–O$\rangle$ = 1.989 Å

$(Nb,Ti)2O_6$ octahedron

(Nb,Ti)2	O3	O3	O7	O7	O6	O6
O3	*1.901(4)*	3.801(7)	2.726(12)	2.732(12)	2.725(6)	2.773(6)
O3	180.0(4)	*1.901(4)*	2.732(12)	2.726(12)	2.773(6)	2.725(6)
O7	89.9(7)	90.1(7)	*1.959(10)*	3.917(17)	2.660(12)	2.914(12)
O7	90.1(7)	89.9(7)	180.0(10)	*1.959(10)*	2.914(2)	2.660(12)
O6	89.0(5)	91.0(5)	84.8(8)	95.2(8)	*1.987(7)*	3.974(10)
O6	91.0(5)	89.0(5)	95.2(8)	84.8(8)	180.0(6)	*1.987(7)*

$\langle$(Nb,Ti)2–O$\rangle$ = 1.949 Å

LaO_{12} polyhedron (CN = 12)

La–O4	2.490(5)	La–O5	$2.6395)\times2$
La–O6	$2.569(4)\times2$	La–O1	2.641(6)
La–O7	2.581(12)	La–O7	2.781(12)
La–O3	$2.627(4)\times2$	La–O3	$2.864(4)\times2$

$\langle$La–O$\rangle$ = 2.658 Å

$Li1O_4$ tetrahedron

Li1	O2	O2	O2
O2	*2.013(16)*	3.697(5)	3.018(4)	3.018(4)
O2	133.3(2)	*2.013(3)*	3.018(4)	3.018(4)
O2	95.1(4)	95.1(4)	*2.075(6)*	4.043(5)
O2	95.1(4)	95.1(4)	153.9(5)	*2.075(14)*

$\langle$Li1–O$\rangle$ = 2.044 Å

$Li2O_4$ tetrahedron

Li2	O2	O2	O2	O2
O2	*2.038(2)*	3.874(5)	3.018(4)	3.018(4)
O2	143.8(2)	*2.038(5)*	3.018(4)	3.018(4)
O2	95.5(2)	95.5(2)	*2.038(5)*	3.874(5)
O2	95.5(2)	95.5(2)	143.8(2)	*2.038(2)*

$\langle$Li2–O$\rangle$ = 2.038 Å

The main bond distances of all the compounds investigated here are given in Tables 7–9. We find the BO_6 octahedra, which form the outer layer of the slabs in $Li_2[A_xB_nO_{3n+1}]$, are characterized by off-centering of the B atoms leading to four equatorial B–O distances of nearly equal length (1.95–1.99 Å), a short B–O (1.78–1.88 Å) bond and a long opposite B–O bond (2.09–2.27 Å). This kind of distortion, leading to long and short bonds along the *c*-axis, is well known in layered perovskites; *e.g.*, values of 1.7 and 2.4 Å are reported for the short and long bonds, respectively.[36,37] For $Li_2La_{1.78}Nb_{0.66}Ti_{2.34}O_{10}$ and $Li_2Sr_2Nb_{3.97}Fe_{0.03}O_{12.97}$, the BO_6 octahedra forming the middle layer are less distorted with the B–O bond lengths in the range 1.90–1.99 Å. In general, for $Li_2La_{1.78}Nb_{0.66}Ti_{2.34}O_{10}$, the $(Nb/Ti)O_6$ octahedra are more distorted compared to the corresponding $(Nb/Fe)O_6$ octahedra in the $Li_2Sr_{0.5n}(Nb,Fe)_nO_{3n+1}$ series, which is as expected since Ti^{4+} is well known to show a larger distortion.[37]

The Sr/La atoms occupy the twelve-coordinated sites in the perovskite cages with the Sr/La–O distances agreeing well with the values in the literature ranging from 2.5 to 2.9 Å. Again,

Table 9 Selected interatomic distances (Å) and angles (°) for $Li_2Sr_2Nb_{3.97}Fe_{0.03}O_{12.97}$

$(Nb,Fe)1O_6$ octahedron						
(Nb,Fe)1	O2	O1	O4	O4	O4	O4
O2	*1.932(16)*	3.898(18)	2.730(13)	2.730(13)	2.730(13)	2.730(13)
O1	180.0(1)	*1.966(6)*	2.821(8)	2.821(8)	2.821(8)	2.821(8)
O4	88.6(8)	91.4(4)	*1.977(1)*	3.952(1)	2.794(1)	2.794(1)
O4	88.6(8)	91.4(4)	177.2(1)	*1.977(1)*	2.794(1)	2.794(1)
O4	88.6(8)	91.4(4)	90.0(1)	90.0(1)	*1.977(3)*	3.952(14)
O4	88.6(8)	91.4(4)	90.0(1)	90.0(1)	177.2(8)	*1.977(3)*
⟨Nb,Fe⟩1–O = 1.967 Å						
$Nb2O_6$ octahedron						
Nb2	O3	O5	O5	O5	O5	O2
O3	*1.864(16)*	2.839(15)	2.839(14)	2.839(14)	2.839(14)	3.996(23)
O5	95.1(9)	*1.984(1)*	3.952(1)	2.794(1)	2.794(1)	2.781(15)
O5	95.1(9)	169.9(1)	*1.984(1)*	2.794(1)	2.794(1)	2.781(15)
O5	95.1(8)	89.6(1)	89.6(1)	*1.984(3)*	3.952(18)	2.781(16)
O5	95.1(8)	89.6(1)	89.6(1)	169.9(1)	*1.984(5)*	2.781(16)
O2	180.0(1)	84.9(8)	84.9(8)	84.9(1)	84.9(9)	*2.132(16)*
⟨Nb2–O⟩ = 1.988 Å						
$Sr1O_{12}$ polyhedron (CN = 12)			$Sr2O_{12}$ polyhedron (CN = 12)			
Sr–O4	2.786(7) × 4		Sr–O1	2.794(1) × 4		
Sr–O2	2.796(1) × 4		Sr–O4	2.821(7) × 8		
Sr–O5	2.725(9) × 4					
⟨Sr1–O⟩ = 2.769 Å			⟨Sr2–O⟩ = 2.812 Å			
LiO_4 tetrahedron						
Li	O3	O3	O3	O3		
O3	*2.049(1)*	3.952(20)	2.998(7)	2.998(7)		
O3	149.3(8)	*2.049(9)*	2.998(7)	2.998(7)		
O3	94.0(4)	94.0(4)	*2.049(4)*	3.952(1)		
O3	94.0(4)	94.0(4)	149.3(3)	*2.049(4)*		
⟨Li–O⟩ = 2.049 Å						

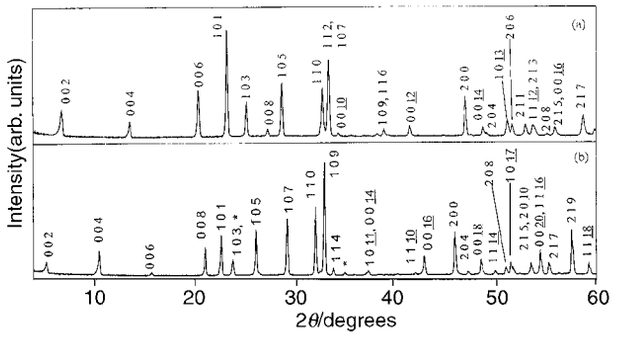

Fig. 8 Powder X-ray diffraction patterns of (a) $Li_2Ca_{1.5}Nb_3O_{10}$ and (b) $Li_2Sr_2(Nb_{3.75}Fe_{0.25})O_{12.75}$. In (b), the asterisks indicate $LiNbO_3$ impurities.

we find the variations in the bond lengths are higher in $Li_2La_{1.78}Nb_{0.66}Ti_{2.34}O_{10}$ in comparison to $Li_2Sr_{0.5n}B_nO_{3n+1}$ (B = Nb, Ta, Fe). In all the phases, the lithium atoms occupy all the distorted tetrahedral sites forming sheets interleaving the perovskite slabs with a Li–O distance of *ca.* 2.0 Å.[27]

We could also prepare $Li_2Ca_{1.5}Nb_3O_{10}$ and $Li_2Sr_2(Nb_{3.75}Fe_{0.25})O_{12.75}$ in bulk and their XRD patterns (Fig. 8) could be clearly indexed on a tetragonal cell (Table 10). It is noteworthy

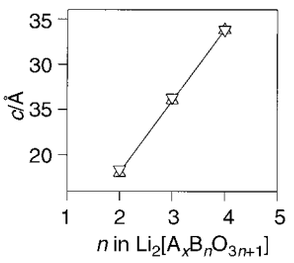

Fig. 9 Plot of *n vs. c* for various phases prepared in the series $Li_2[A_xB_nO_{3n+1}]$. The upward and downward triangles represent A = Sr, B = Nb and A = La, B = Ti, respectively.

Table 10 Composition, *n*, and lattice parameters of various compounds prepared in the series $Li_2[A_{0.5n}B_nO_{3n+1}]$

Composition	*n*	Vacancy in the A site	Lattice parameter/Å	
			a	*c*
$Li_2SrNb_2O_7$ [a]	2	0	—	18.011(3)
$Li_2SrTa_2O_7$	2	0	3.9499(2)	18.200(3)
$Li_2Sr_{1.5}Nb_3O_{10}$ [b]	3	0.25	3.953(2)	26.041(5)
$Li_2Ca_{1.5}Nb_3O_{10}$	3	0.25	3.8818(9)	26.232(7)
$Li_2Sr_2Nb_{3.75}Fe_{0.25}O_{12.75}$	4	0.33	3.9609(7)	33.821(6)

[a]Crystallizes in orthorhombic cell with $a = 5.5939(1)$, $b = 5.6013(1)$, $c = 18.011(3)$ Å. See text for details. [b]Reported by us in ref. 25.

that the *c*-parameters of various members in the Li–Sr–Nb–Fe–O and Li–La–Nb–Ti–O systems vary linearly with the value of *n* (Fig. 9).

Interestingly, we find that, with the formation of the $n = 4$ member, $Li_2Sr_2Nb_{3.97}Fe_{0.03}O_{12.97}$, the compounds of the Li–A–B–O systems (A = Ca, Sr; B = Nb, Ta) form a new family of layered perovskites with general formula $Li_2A_{0.5n}B_nO_{3n+1}$ (Table 10). The significance of this new family is twofold:

1. The ratio of the A to B cations remains the same throughout the series independent of *n*.

2. As *n* increases, the number of vacancies in the twelve-coordinated sites increases.

The importance of the first factor is that it is possible to prepare compounds with various *n* values for a fixed set of A and B cations in the series by controlling the amount of lithium and temperature conditions, unlike the compounds of the DJ and RP series of the type $A'_x[A_nB_{n+1}O_{3n+1}]$ ($x = 1$ and 2 for the respective phases), which are restricted to a particular value of *n* for a set of A and B cations. The consequence of second factor is instantly seen from the values of conductivity of various phases. Our results§ indicate that the conductivity values increase directly with the increase in *n* (*i.e.*, with increase in the vacant A sites and hence allowing the Li^+ ions to pass through the perovskite slabs); moving from $n = 2$

§To be published elsewhere.

(1.95×10^{-7} S cm^{-1}, for $Li_2SrNb_2O_7$ at 250 °C) to $n=3$ (4.9×10^{-6} S cm^{-1}, for $Li_2Sr_{1.5}Nb_3O_{10}$ at 280 °C)[25] and then to $n=4$ (9.4×10^{-5} S cm^{-1}, for $Li_2Sr_2Nb_{3.75}Fe_{0.25}O_{12.75}$ at 257 °C) we see at least a 20-fold increase in the values of conductivity, with same set of A and B cations.‖

Conclusions

We have synthesized several members of the family $Li_2[A_xB_nO_{3n+1}]$ (A = La, Sr, Ca; B = Nb, Ta, Ti, Fe) for the first time. While the structures of the $n=2$ members, $Li_2SrNb_2O_7$ and $Li_2SrTa_2O_7$, are similar to that of the RP phases, the higher members, $Li_2La_{1.78}Nb_{0.66}Ti_{2.34}O_{10}$, $Li_2Ca_{1.5}Nb_3O_{10}$ ($n=3$), and $Li_2Sr_2Nb_{3.97}Fe_{0.03}O_{12.97}$ ($n=4$) show vacancies in the twelve-coordinated A sites. The electron microscopic studies, although in agreement with the X-ray diffraction results, show the presence of super-cell reflections, defects or intergrowth structures in these phases. Significantly, with our previous results on $Li_2Sr_{1.5}Nb_3O_{10}$ and present work on $n=2$ and 4 members in the Li–A–B–O system (A = Ca, Sr; B = Nb, Ta, Fe), we have demonstrated the formation of a new family of layered perovskites $Li_2A_{0.5n}B_nO_{3n+1}$, where various members can be formed with the same set of A and B cations. Also, an enhancement of lithium ion conduction with n is evidenced for these new oxides as a consequence of an increase in the number of vacant A sites.

Acknowledgements

We thank Dr V. Maisonneuve (Laboratoire des Fluorures, Université du Maine) and Dr Piffard (IMN, Nantes) for their help in collecting the single X-ray diffraction data. One of us (N. S. P. B.) thanks Région des Pays de la Loire and CNRS for financial support.

References

1 S. N. Ruddlesden and P. Popper, *Acta Crystallogr.*, 1957, **10**, 538; 1958, **11**, 54.
2 A. R. Armstrong and P. A. Anderson, *Inorg. Chem.*, 1994, **33**, 4366.
3 A. J. Wright and C. Greaves, *J. Mater. Chem.*, 1996, **6**, 1823.
4 M. Dion, M. Ganne and M. Tournoux, *Mater. Res. Bull.*, 1981, **16**, 1429.
5 M. Dion, M. Ganne and M. Tournoux, *Rev. Chim. Miner.*, 1986, **23**, 61.
6 A. J. Jacobson, J. W. Johnson and J. T. Lewandowski, *Inorg. Chem.*, 1985, **24**, 3727.
7 J. Gopalakrishnan, V. Bhat and B. Raveau, *Mater. Res. Bull.*, 1987, **22**, 413.
8 M. A. Subramanian, J. Gopalakrishnan and A. W. Sleight, *Mater. Res. Bull.*, 1988, **23**, 837.
9 R. A. Mohan Ram and A. Clearfield, *J. Solid State Chem.*, 1991, **94**, 45.
10 S. Uma and J. Gopalakrishnan, *Chem. Mater.*, 1994, **6**, 907.
11 B. Aurivillius, *Ark. Kemi*, 1949, **1**, 463, 499; 1950, **2**, 519.
12 S. Uma, A. R. Raju and J. Gopalakrishnan, *J. Mater. Chem.*, 1993, **3**, 709.
13 A. J. Jacobson, J. T. Lewandowski and J. W. Johnson, *J. Less-Common Met.*, 1984, **21**, 92.
14 A. J. Jacobson, J. W. Johnson and J. T. Lewandowski, *Mater. Res. Bull.*, 1987, **22**, 45.
15 J. Gopalakrishnan and V. Bhat, *Inorg. Chem.*, 1987, **26**, 4299.
16 K. Park and S.-H. Byeon, *Bull. Korean Chem. Soc.*, 1996, **17**, 168.
17 K. Toda, Y. Kameo and M. Fujimoto, *J. Ceram. Soc. Jpn. Int. Ed.*, 1994, **102**, 735.
18 K. Domen, J. Yoshimura, T. Sekine, A. Tanaka and T. Onishi, *Catal. Lett.*, 1990, **4**, 339.
19 S. Ikeda, A. Tanaka, M. Hara, J. N. Kondo, K. Maruya and K. Domen, *Microporous Mater.*, 1997, **9**, 253.
20 S. Ikeda, M. Hara, J. N. Kondo, K. Domen, H. Takahashi, T. Okubo and M. Kakihana, *Chem. Mater.*, 1998, **10**, 72.
21 Y. Moritomo, A. Asamitsu, H. Kuwahara and Y. Tokura, *Nature*, 1996, **380**, 141.
22 R. Seshadri, C. Martin, M. Herien, B. Raveau and C. N. R. Rao, *Chem Mater.*, 1997, **9**, 270.
23 P. D. Battle, M. A. Green, N. S. Laskey, J. E. Millburn, L. Murphy, M. J. Rosseinsky, S. P. Sullivan and J. F. Vente, *Chem. Mater.*, 1997, **9**, 552.
24 Y. Takano, S. Takayanagi, S. Ogawa, T. Yamadaya and N. Mori, *Solid State Commun.*, 1997, **103**, 215.
25 N. S. P. Bhuvanesh, M. P. Crosnier-Lopez, O. Bohnke, J. Emery and J. L. Fourquet, *Chem. Mater.*, 1999, **11**, 634.
26 M. P. Crosnier-Lopez, H. Duroy and J. L. Fourquet, *Mater. Res. Bull.*, 1999, **34**, 179.
27 M. P. Crosnier-Lopez, N. S. P. Bhuvanesh, H. Duroy and J. L. Fourquet, *J. Solid State Chem.*, 1999, **145**, 136.
28 J. Rodriguez-Carvajal, FULLPROF program: Rietveld Pattern Matching Analysis of Powder Patterns, ILL Grenoble, 1990.
29 M. Sato, T. Jin and H. Ueda, *Chem. Lett.*, 1994, 161.
30 N. Floros, C. Michel, M. Hervieu and B. Raveau, *J. Mater. Chem.*, 1999, **9**, 3101.
31 G. M. Sheldrick, SHELX-93: A Program for the Refinement of Crystal Structures from Diffraction Data, University of Göttingen, Germany, 1993.
32 *International Tables for X-Ray Crystallography*, Kynoch Press, Birmingham, 1974, vol. IV.
33 T. Suzuki, *Acta Crystallogr.*, 1960, **13**, 279.
34 M. A. McCoy, R. W. Grimes and W. Lee, *Philos. Mag. A*, 1997, **75**, 833.
35 K. Chiba, N. Ishizawa, Y. Nagai and S. Oishi, *Solid State Ionics*, 1998, **108**, 179.
36 M. Kunz and I. D. Brown, *J. Solid State Chem.*, 1995, **115**, 395.
37 N. S. P. Bhuvanesh and J. Gopalakrishnan, *J. Mater. Chem.*, 1997, **7**, 2297 and references therein.

Paper 9/03720I

‖For $n=4$, we have used $Li_2Sr_2(Nb_{3.75}Fe_{0.25})O_{12.875}$ for comparison, where the Nb^{5+} is substituted, to a small extent by Fe^{3+}.